WELDING RESEARCH

SUPPLEMENT TO THE *WELDING JOURNAL*, APRIL 1989

Sponsored by the American Welding Society and the Welding Research Council

Stress-Relief Cracking of a Copper-Containing HSLA Steel

An experimental low-carbon, age-hardening steel appears to be more susceptible to stress-relief cracking than the higher-carbon HY-80 steel

BY J. P. BALAGUER, Z. WANG AND E. F. NIPPES

ABSTRACT. The stress-relief cracking susceptibility of an age-hardening alloy steel and the effects of mechanical constraint in the weld HAZ were investigated. Stress-relief cracking tests were performed on simulated weld heat-affected zones of HY-80, a quench-and-tempered steel, and HSLA-100, an experimental age-hardening copper-containing steel, at temperatures of 575° and 625°C (1067° and 1157°F) and stress levels of 274 to 550 MPa (40 to 80 ksi). Measurements of flow stress in the coarse-grained HAZ of HSLA-100 indicated that a substantial increase in flow stress occurs during the transformation of unstable austenite to lower-temperature microconstituents. Approximately 30% of the room-temperature yield strength is attained only after approximately 50% of the microstructural transformation is complete. Based on these data, a thermomechanical (rather than just a thermal) simulation test was developed to model the effect of stress and thermal transients on the stress-relief cracking susceptibility of these steels. The imposition of mechanical constraint on the cooling portion of the weld thermal cycle resulted in a slight increase in HAZ hardness and stress-relief cracking susceptibility of the HSLA-100 steel. The strain-to-failure in stress-rupture tests of HSLA-100 was approximately half that of HY-80; stress-rupture ductilities for HSLA-100 were less than 10% for all test conditions. Failure of the HY-80 and HSLA-100 steels occurred by classical low-ductility intergranular fracture. Several models of low-ductility intergranular fracture are examined with respect to the results of this investigation.

J. P. BALAGUER is a Research Assistant and E. F. NIPPES is a Professor of Metallurgy in the Materials Engineering Department, Rensselaer Polytechnic Institute, Troy, N.Y. Z. WANG is a Research Assistant in the Department of Mining and Metallurgical Engineering at McGill University and an Associate Engineer at the Xing Hua Machinery Factory, Beijing, Peoples Republic of China.

Paper presented at the 69th Annual AWS Meeting, held April 17-22, 1988, in New Orleans, La.

KEY WORDS

Stress-Relief Cracking
Cu-Containing Steels
HSLA-100 Steel
Crack Susceptibility
Mechanical Constraint
Stress-Thermal Model
Intergranular
Aging Response
Reheat Cracking
HY-80 Steel

Introduction

Stress-relief cracking (also known as strain-age cracking and reheat cracking) is prevalent in high-strength structural steels. It occurs during postweld heat treatment (PWHT) of welds, in the temperature range of 482° to 677°C (900° to 1250°F), to relieve residual stresses. Meitzner (Ref. 1), in a comprehensive review of stress-relief cracking (SRC) in weldments, stated that SRC was associated with:

1) Precipitation-hardening materials only.

2) Intergranular failure with little or no evidence of deformation.

3) The coarse-grained region of the weld HAZ.

In-service stress-relief cracking is often observed in welded pressure-vessel steels as well as nickel-base superalloys (Refs. 2, 3). Precipitation-strengthened HSLA steels, while not normally subjected to PWHT, have been shown to be susceptible to SRC (Ref. 4).

In low-alloy steels, the mechanism of SRC is commonly thought to be related to the intragranular precipitation of alloy carbides (such as V_4C_3 or Mo_2C in Cr-

Mo-V steels) upon high-temperature exposure after welding (Ref. 1). This precipitation strengthens the grain interiors, thus, creep deformation associated with stress relief is concentrated at the grain boundaries. As a result of grain growth in the HAZ near the fusion line, the grain-boundary area is reduced, and creep deformation is concentrated over a relatively small area. Deformation is concentrated at the grain boundaries until wedge-type (triple-point) or cavitation-type cracks are initiated (Ref. 1). In the presence of residual or applied stresses, these creep-initiated cracks propagate until failure occurs. Dix and Savage (Ref. 2) have proposed a similar mechanism for strain-age cracking in nickel-base superalloys. However, a recent study by Sun, *et al.* (Ref. 5), has shown that trace impurities, not carbide-forming elements, were responsible for SRC in a Mn-Mo-Ni-Cr pressure-vessel steel, ASTM A508 Class 2.

Shin and McMahon (Ref. 6), in a study of a Mn-Mo-Ni-Cr pressure-vessel steel (ASTM A508 Class 2), identified two distinct modes of stress-relief cracking in notched specimens. At low stresses, microcracking initiated by a cavitation-mode mechanism and cavity growth was controlled primarily by plastic flow. At high stresses, a transition to a brittle mode of cracking occurred; this failure mode resulted in an intergranular faceted fracture surface. The brittle fracture mode was associated with the solutionizing of sulfide inclusions and reprecipitation of sulfur on the grain boundaries. The authors proposed that the sulfur in solution diffused to the crack tip, attained a critical concentration, and caused decohesion and crack growth. This proposed mechanism is similar to the hydrogen embrittlement mechanism proposed by Troiano (Ref. 7). This mechanism of stress-driven solute enrichment of crack tips, *e.g.*, by S, has been theoretically proven by Hippsley, Rauh and Bullough (Ref. 8). Most recently, the segregation of S to intergranular facets in the presence of hydrostatic stresses and the role of S as the primary embrittling species have been confirmed experimentally by Lewandowski, *et al.* (Refs. 9, 10), and Sun, *et al.* (Ref. 5). Sun, *et al.* (Ref. 5), has shown that S acts synergistically with other trace impurities, including B, to cause intergranular embrittlement of low-alloy steels and that addition of P to S-containing steel can actually reduce SRC susceptibility. Druce, Gage and Jordan (Ref. 11) have maintained that, in Mn-Mo-Ni pressure-vessel steels (ASTM 533B and 508), segregation of P to prior austenite grain boundaries was the primary cause of grain-boundary embrittlement upon aging.

It is well known that high-temperature excursions experienced in the coarse-grained HAZ may result in carbide dissolution and reprecipitation on grain boundaries. Emmer, Clauser and Low (Ref. 12) have reported that grain-boundary carbides decrease the boundary cohesive strength; this provides an easy intergranular fracture path. There is no agreement, however, on whether precipitate-free zones adjacent to grain boundaries increase or decrease ductility during stress relief (Ref. 1). It is well recognized that adsorption of segregated impurities at the interfaces of grain-boundary particles may promote SRC (Ref. 1). Meitzner (Ref. 1) has observed that Cu and other trace elements in steel have a deleterious effect on SRC susceptibility for long-time (cavitation-mode) failures, but have little effect on short-time (wedge-type cracking) failures.

Recently, Lundin, Menon and Chen (Ref. 4) have suggested that intragranular precipitation of Cu-rich particles in A-710 steel during PWHT promotes SRC in the grain-coarsened (1316°C/2400°F peak temperature) HAZ. Cracking was not observed, however, in the grain-refined (954°C/1750°F peak temperature) or the partially refined (788°C/1450°F peak temperature) regions of the weld HAZ. The absence of cracking was ascribed to increased grain-boundary area; as a result, there was a greater accommodation of creep strains and a decreased fraction of solutionized carbides and precipitates. This is in direct contrast to Shin and McMahon (Ref. 6), who, in a study of a Mn-Mo-Ni-Cr pressure-vessel steel, have shown that SRC was not dependent on prior austenite grain size but on the amount by which the HAZ simulation peak temperature exceeded a critical value for SRC.

The role of strain in precipitation associated with SRC during PWHT has not been well documented. However, at least two separate investigations have shown that strain increases precipitation (Ref. 13) and hardness (Ref. 14) during aging of ferritic materials. Rosenstein (Ref. 15) has investigated the effects of low-temperature strain and relaxation-induced creep strain on the toughness of a 5 Ni-Cr-Mo-V steel. The Charpy V-notch impact toughness of prestrained and stress-relieved samples was compared with that of samples subjected to stress relief only. Both low-temperature and creep strains, applied prior to stress-relief treatment, were found to degrade impact toughness.

Previously, two general types of tests have been utilized to evaluate SRC susceptibility for low-alloy steels: 1) indirect weldability tests, such as Gleeble HAZ simulation (Refs. 4, 14, 16–18), and 2) direct weldability tests, such as the Lehigh restraint test (Refs. 14, 17) and the Y-groove and C-ring tests (Ref. 4).

While HAZ simulation tests for SRC susceptibility effectively reproduce HAZ microstructures, they often do not replicate the mechanical constraint present in the weld HAZ on cooling from the peak temperature.

SRC/HAZ simulation tests have been utilized in at least three forms:

1) Slow strain-rate tensile tests of unnotched HAZ simulation specimens at the stress-relief temperature (Refs. 14, 17, 18).

2) Stress-relaxation tests of HAZ simulation notched specimens at the stress-relief temperature (Ref. 14).

3) Stress rupture tests of unnotched HAZ simulation specimens at the stress-relief temperature (Refs. 4, 16).

The strain-to-failure (ϵ_f or %RA) is used as a measure of SRC susceptibility for HAZ simulation tests. Meitzner and Pense (Ref. 14) have shown that low-tensile ductility at 593°C (1100°F) and short rupture life in notched stress-relaxation tests correlate well with stress-relief cracking in weld restraint tests.

All three of these tests are lacking in an important feature: the increase in residual stress that occurs in the HAZ on cooling from the peak temperature. Also, Tests 1 and 3 do not simulate the decrease in residual stress that accompanies plastic deformation during stress-relief treatment. Duvall and Owczarski (Ref. 17) have shown that stress-relaxation tests can be used to simulate the change in mechanical constraint, which occurs upon PWHT of nickel-base superalloys. The failure mode observed in these tests was similar to that produced in restrained welds. Visbisky (Ref. 16) has reported results from SRC/HAZ simulation tests of Cr-Mo-V and Ni-Cr-Mo-V steels in which a stress was superimposed on cooling from the peak temperature; however, the details of this technique and the effect of stresses on precipitation in the weld HAZ have not been reported in the literature.

The object of this investigation was to examine the stress-relief cracking susceptibility of an experimental age-hardening alloy steel and to examine the effects, if any, of mechanical constraint on stress-relief cracking susceptibility of this steel. Additionally, proposed mechanisms of stress-relief embrittlement were to be examined, critically, in light of the results of this and other investigations.

Materials and Experimental Procedure

The materials used in this investigation were HY-80, a high yield strength, quench-and-tempered steel, and HSLA-100, an experimental, low-carbon, age-hardening, copper-containing steel (based on ASTM A710) designed to meet mechanical-property specifications for HY-100. The relatively high strength of

Table 1—Chemical Composition of Steels Used in This Investigation (wt-%)

Heat	C	Mn	Ni	Mo	Cr	Ti	Nb	N	B	Cu	Al	Si	P	S
HSLA-100	0.03	0.92	3.45	0.52	—	0.01	0.03	0.010	(a)	1.58	(a)	0.26	0.018	0.005
HY-80	0.18	0.30	2.97	0.41	1.68	(a)	—	0.007	(a)	0.03	(a)	0.20	0.018	0.013

(a) Not analyzed.

Table 2—Mechanical Properties of Materials Used in This Investigation

Steel Type	Thick. mm (in.)	UTS MPa (ksi)	YS MPA (ksi)	% Elong. (in 25 mm)
HY-80	50 (2.0)	745 (108)	607 (88)	25
HSLA-100	25 (1.0)	835 (121)	807 (117)	24

these HSLA steels results from the age-hardening effect of Cu in Fe. The presence of Cu-rich precipitates in a low-carbon (< 0.07 wt-%) matrix results in a relatively high toughness/yield strength ratio. The offsetting effects of grain refinement and precipitation strengthening can increase yield strength without changing the DBTT as measured by fracture toughness testing (Ref. 19). Prior to testing, the HSLA-100 was heat treated using the guidelines of ASTM A710 specifications (Ref. 20). The details of the heat treatment used are discussed in the next section. HY-80 steel was supplied in the heat-treated (quench-and-tempered) condition. The chemical composition and mechanical properties of these alloys are listed in Tables 1 and 2.

Weld HAZ simulation and stress-relief cracking tests were performed on a Gleeble 1500 thermomechanical testing machine. The simulated HAZ produced in 6.35-mm (0.25-in.) diameter test specimens was equivalent to that produced 11.4 mm (0.45 in.) from the weld centerline in a 3.9 kJ/mm (100 kJ/in.) weld in 25-mm (1.0-in.) thick plate fabricated with 93°C (200°F) preheat. These parameters resulted in a peak temperature of 1315°C (2400°F) and a $t_{800\text{-}500}$ of 33.1 s.

Two types of SRC tests were utilized in this study:

Type 1 (termed as no-load-on-cooling) is the classical SRC/HAZ simulation test described previously. In this test, the specimen was subjected to a weld thermal cycle, cooled to room temperature, stressed to a predetermined level, and then reheated to the stress-relief temperature. The time to failure (t_f) at a given stress level was used as a measure of SRC susceptibility.

Type 2 (termed as load-on-cooling) is a stress-rupture test modified to include some degree of the mechanical constraint normally present in a weld HAZ. In this test, the specimen was first subjected to a weld thermal cycle. Upon cooling to a temperature just below the beginning of transformation (approximately 400°C), a stress equivalent to the yield strength of the material at this temperature was applied. As the specimen continued to cool from 400°C to room temperature, the stress was continuously increased to simulate the increase in residual stress in the weld HAZ. After cooling to room temperature, the stressed specimen was reheated to the stress-relief temperature in 30 s. During specimen heating, the stress was adjusted to the appropriate value for a particular stress-rupture test. Schematic diagrams of time-temperature-stress relationships for Type 1 and Type 2 tests are shown in Fig. 1.

No-load-on-cooling (Type 1) tests were conducted on HY-80 and HSLA-100 at 625°C (1157°F). Selection of test temperature for Type 1 tests was based upon suggested stress-relief temperatures for HY-80; the specified stress-relief temperature range for this steel is 593° to 621°C (1100° to 1150°F) (Ref. 21). Load-on-cooling (Type 2) tests were conducted on HSLA-100, and were performed at temperatures of 575° and 625°C (1067° and 1157°F). Test temperatures for Type 2 tests were selected at increments of 50° and 100°C (90° and 180°F) below the aging temperature for HSLA-100 (selection of aging temperature is discussed in the next section). Based on measurements of weld HAZ yield strengths, stresses of 274 to 550 MPa (40 to 80 ksi) were used for stress-rupture tests. All tests, including weld HAZ simulation, were conducted in air.

After SRC testing, specimens were sectioned and prepared for optical microscopy using standard metallographic techniques. In order to preserve the fracture surfaces, several specimens were nickel plated prior to metallographic preparation. Chemical etchants of either 2% Nital or 2% Picral were used to reveal microstructural details. Fracture surfaces of SRC test specimens were also examined using the scanning electron microscope (SEM). Microhardness testing was performed using a Vickers diamond pyramid indenter with a 1-kg load.

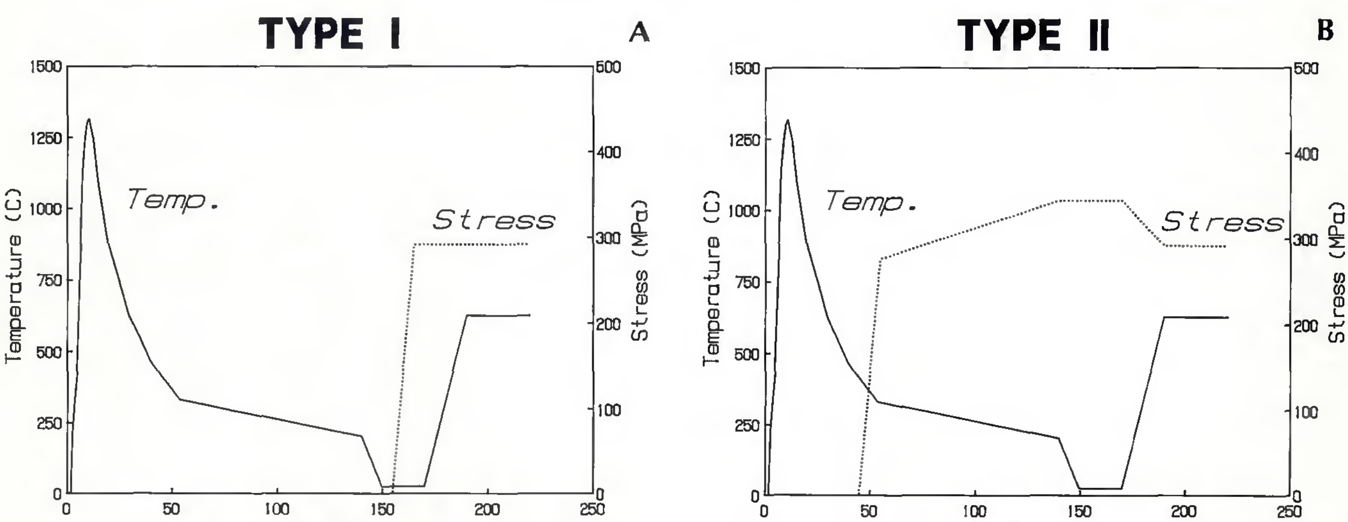

Fig. 1—Schematic representation of Type 1 (A) and Type 2 (B) simulated HAZ stress-relief cracking tests used in this investigation

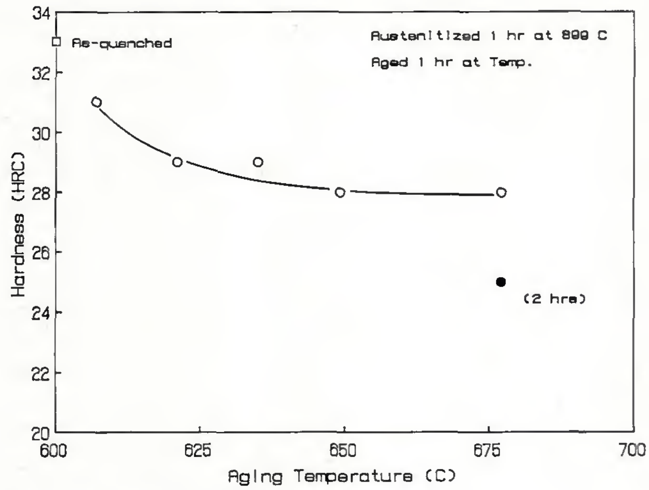

Fig. 2 — Aging response of HSLA-100

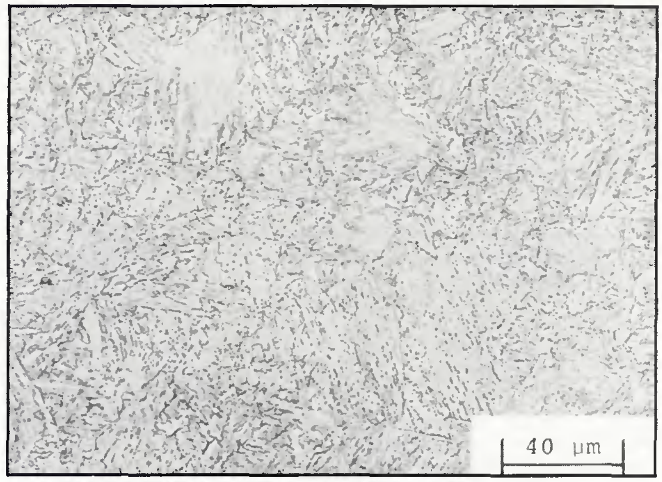

Fig. 3 — Photomicrograph of HSLA-100 in the austenitized and aged condition, 2% Nital etch, 500X

Results

Aging Response

Samples of HSLA-100 were austenitized for 1 h at 899°C (1650°F), water quenched, and aged for 1 h at temperatures of 607°, 621°, 635°, 649° and 677°C (1125°, 1150°, 1175°, 1200° and 1250°F). The hardness of these samples was measured; the aging response of HSLA-100 is shown in Fig. 2. Optimum mechanical properties (see Table 2) were achieved with the following heat treatment schedule: austenitize at 899°C for 1 h, water quench, age at 677°C for 2 h, and air cool. The microstructure produced by this heat treatment is shown in Fig. 3; the microhardness of this structure was HV 263 (HRC 25). All HSLA-100 stress-relief-cracking test specimens were heat treated according to this schedule prior to HAZ simulation.

Weld HAZ Simulation

The coarse-grained HAZ microstructures produced in HY-80 and HSLA-100 by weld simulation are shown in Figs. 4 and 5, respectively. The hardness of the heat-affected zones in HY-80 and HSLA-100 were HV 421 and 284, respectively. The comparatively low HAZ hardness of HSLA-100 is a result of its low carbon content (0.03 wt-%) and is an indicator of its potentially high resistance to hydrogen-induced cracking. In a separate investigation, to be published at a later date (Ref. 22), it was found that the coarse-grained HAZ hardness of HSLA-100 was only mildly dependent on $t_{800-500}$. One specimen of HSLA-100 was subjected to the load-on-cooling described in the previous section, but did not undergo stress-relief treatment. This specimen was metallographically sectioned and hardness tested. No difference in the microstructure of the specimen cooled under mechanical constraint and that shown in Fig. 5 could be resolved with optical microscopy. However, the microhardness was slightly elevated (HV 305 versus HV 284 for no-load-on-cooling). This increase in hardness was ascribed to the stress-induced effect on the diffusion of Cu and on the precipitation of the Cu-rich zones.

In order to determine the appropriate stress levels for SRC testing, the flow stress of the coarse-grained HAZ of HSLA-100 was measured using the Gleeble. The 0.2% offset yield strength measured at 625°C on cooling from a peak temperature of 1315°C was 30 MPa (4.3 ksi). After cooling to room temperature and reheating to 625°C, the measured yield strength was 331 MPa (47.9 ksi). Dilatation measurements made during HAZ simulation indicated bainite start (B_s) and bainite finish (B_f) temperatures of approximately 470° and 345°C (878° and 653°F), respectively. Additional experiments were performed to determine the force required to produce a constant strain of 1 to 2% on cooling from the peak temperature. A sudden increase in force required to maintain a constant strain was observed at approximately 420°C (788°F).

These data suggest that the metastable low-carbon austenite present on cooling from the peak temperature to 625°C has a relatively low flow stress. Because plastic flow would occur easily at these temperatures, residual stresses in the

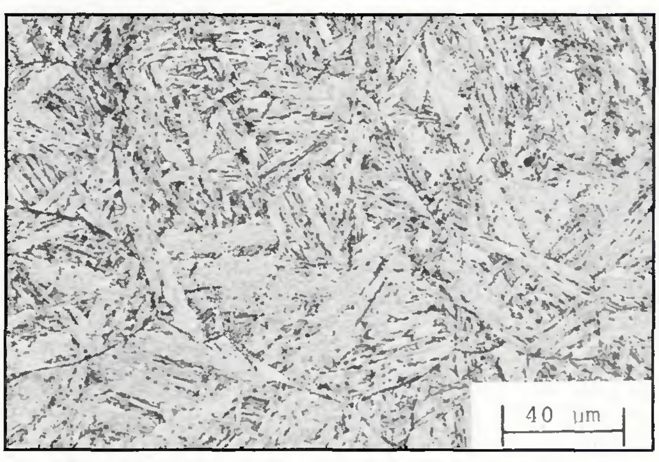

Fig. 4 — Photomicrograph of the coarse-grained HAZ in HY-80, 2% Picral etch, 500X

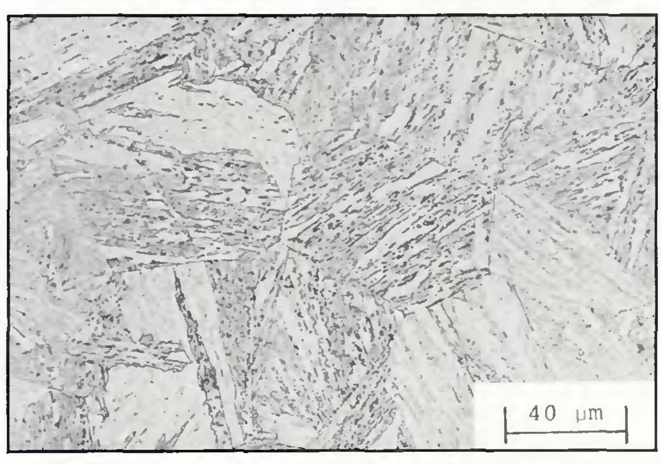

Fig. 5 — Photomicrograph of coarse-grained HAZ in HSLA-100, 2% Nital etch, 500X

weld could not increase significantly in magnitude until the bulk of the austenite had transformed. Therefore, it was determined that in Type 2 tests, a load simulating the residual stress of the weld would be applied only after transformation to lower-temperature microconstituents was at least 50% complete. While this obviously is not a completely accurate simulation of the thermomechanical history of the HAZ, it represents an important step in more accurately simulating the HAZ microstructure and stress state for age-hardened alloy steels.

Stress-Relief Cracking

The results of all stress-relief cracking tests conducted in this investigation are summarized in Table 3. The strain-to-failure (ϵ_f) results for 625°C tests, as a function of time-to-failure (t_f), are shown in Fig. 6. The ϵ_f of both Type 1 and Type 2 tests of HSLA-100 appeared to increase as t_f decreased. The curve shown in Fig. 6 is a second-order polynominal regression fit of both Type 1 and Type 2 data for HSLA-100. There appeared to be no discernible difference in the ϵ_f of HSLA-100 subjected to Type 1 and Type 2 tests. The values of ϵ_f measured for HY-80 were somewhat higher than those measured for HSLA-100 at similar stresses.

The rupture stress (σ) versus t_f results for Type 1 stress-relief cracking tests of HY-80 at 625°C are shown in Fig. 7A. Also shown in Fig. 7A are the results of Type 1 and 2 tests of HSLA-100 at 625°C. These results indicate that, at $t_f < 1$ min, HSLA-100 loaded on cooling was slightly more susceptible to stress rupture failure at 625°C than HSLA-100 loaded after cooling to room temperature. At $t_f > 1$ min, loading on cooling had little effect on t_f at a given stress level.

It is interesting to note that, for similar welding (3.9 kJ/mm, 1315°C peak temperature) and loading (Type 1 test) conditions, HSLA-100 was more susceptible to SRC than HY-80. At stresses of approximately 335 MPa (48.9 ksi) and 455 MPa (65.5 ksi), the t_f for HY-80 was 80 to 85% greater than that measured for HSLA-100. It should also be noted that these stresses represent 61 and 82% of the minimum specified yield strength of HY-80 versus only 49 and 66% of the minimum specified yield strength of HSLA-100. As the primary focus of this investigation was the HSLA-100 steel, no Type 2 tests were performed on HY-80; therefore, no comparisons between the alloys could be made for cooling under mechanical constraint.

The results of Type 2 tests for HSLA-100 at temperatures of 575° and 625°C are shown in Fig. 7B. The lines in Fig. 7B are linear-regression fits; the linear correlation coefficients are also included in the graph. There appears to be a change in the mechanism of failure indicated by a change in slope for HSLA-100 data at 625°C. The change in slope occurs at a stress of 400 MPa (58 ksi), approximately 58% of the specified yield strength of HSLA-100, and a t_f of 1 min. It should also be noted that the slope of the log σ versus log t_f lines, particularly at $t_f < 1$ min, is relatively low. Therefore, a slight increase in residual stress could produce a relatively large decrease in t_f.

Table 3—Stress-Relief Cracking Test Results

Steel	Test Type	Temperature °C	σ MPa (ksi)	ϵ_f	t_f (min)
HY-80	1	625	339 (49.1)	0.140	18.25
HY-80	1	625	381 (55.2)	0.081	7.15
HY-80	1	625	393 (57.0)	0.158	2.30
HY-80	1	625	458 (66.4)	0.073	1.25
HSLA-100	1	625	334 (48.4)	0.040	2.58
HSLA-100	1	625	412 (59.7)	0.024	1.10
HSLA-100	1	625	453 (65.7)	0.065	0.23
HSLA-100	1	625	495 (71.7)	0.048	0.08
HSLA-100	2	625	274 (39.7)	0.032	11.73
HSLA-100	2	625	275 (39.9)	0.024	13.22
HSLA-100	2	625	316 (45.8)	0.032	4.98
HSLA-100	2	625	396 (57.4)	0.032	1.27
HSLA-100	2	625	428 (62.0)	0.048	0.37
HSLA-100	2	625	433 (62.8)	0.081	0.28
HSLA-100	2	625	449 (65.1)	0.065	0.10
HSLA-100	2	575	386 (55.9)	0.040	19.88
HSLA-100	2	575	435 (63.0)	0.032	18.30
HSLA-100	2	575	485 (70.3)	0.065	2.90
HSLA-100	2	575	503 (72.9)	0.073	4.40
HSLA-100	2	575	550 (79.7)	0.089	1.83

Microstructural Analysis

Photomicrographs of cross-sections from HY-80 and HSLA-100 tested under similar conditions (no-load-on-cooling, 625°C, 455 and 497 MPa) are shown in Figs. 8 and 9 at 50X. There was a considerable amount of secondary cracking evident in the HY-80 specimen shown in Fig. 8. Little secondary cracking was observed in the HSLA steel tested with no-load-on-cooling and shown in Fig. 9. A specimen of HSLA-100, a cross-section of which is shown in Fig. 10, was tested under similar conditions but with a load-on-cooling. This specimen showed only slightly more secondary cracking than the HSLA-100 specimen tested with no-load-on-cooling shown in Fig. 9. Another HSLA-100 specimen, tested at 625°C with a load-on-cooling but with a lower stress (276 MPa), displayed a greater amount of secondary cracking than that observed in more highly stressed specimens. A cross-section of this specimen is shown in Fig. 11.

Predominantly intergranular crack paths were observed for both primary (fracture surface) and secondary cracking in all tests, with most cracking occurring perpendicular to the tensile axis. Figure 12 is a higher-magnification (1000X) photomicrograph of a secondary crack in the Type 2 HSLA-100 specimen shown previously in Fig. 10. The crack path was primarily intergranular along prior-austenite grain boundaries; a small amount of transgranular cracking was evident near the triple points as seen in the lower right of the photomicrograph.

Figures 13 and 14A are SEM fracto-

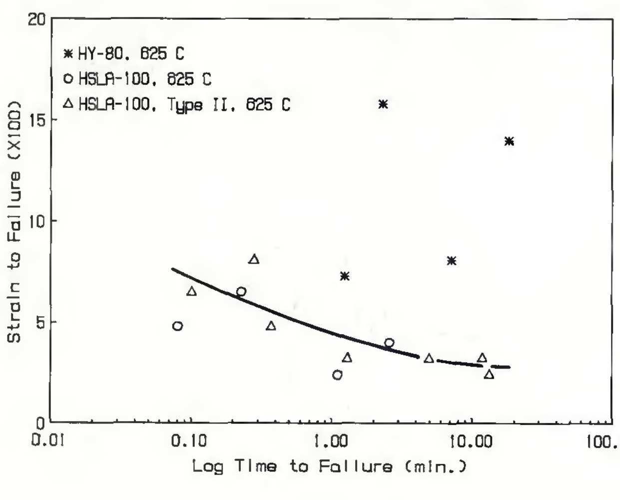

Fig. 6 — ϵ_f versus log t_f for 625°C stress-relief cracking tests of HY-80 and HSLA-100

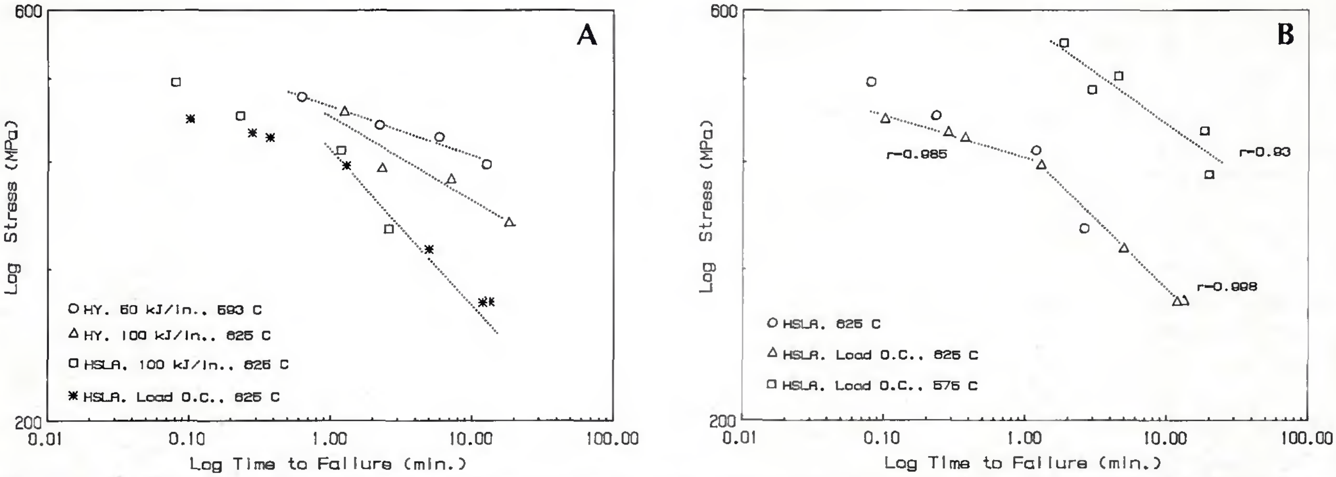

Fig. 7 — A — Log σ versus log t_f for stress-relief cracking tests of HY-80 and HSLA-100 at 625°C; B — Log σ versus Log t_f for stress-relief cracking tests of HSLA-100 at 575° and 625°C

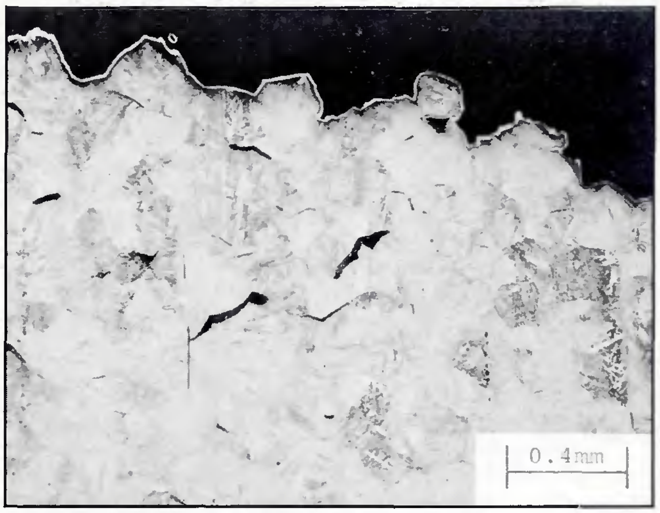

Fig. 8 — Photomicrograph of nickel-plated fracture surface of HY-80 specimen tested at 625°C with no-load-on-cooling (455 MPa, t_f = 1.25 min), 2% Nital etch, 50X

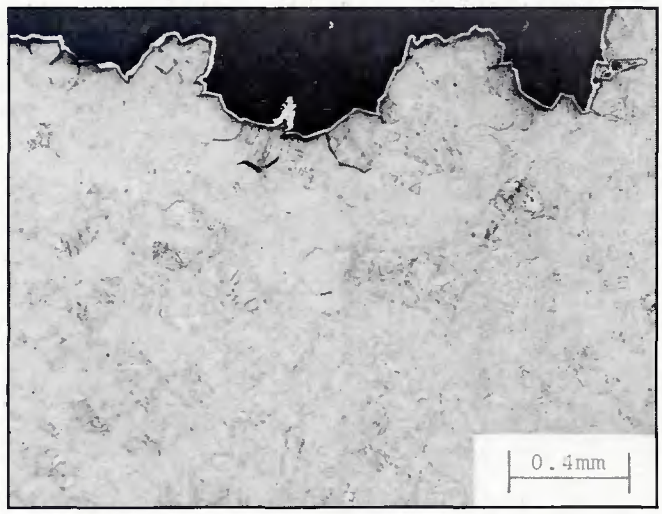

Fig. 9 — Photomicrograph of nickel-plated fracture surface of HSLA-100 specimen tested at 625°C with no-load-on-cooling (497 MPa, t_f = 5 s), 2% Nital, 50X

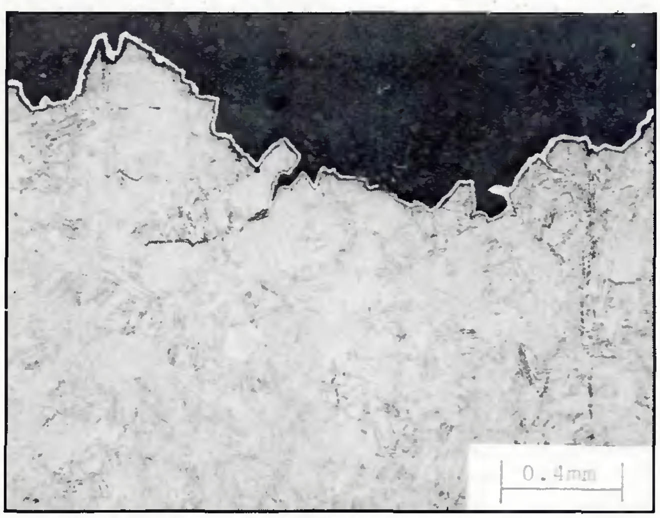

Fig. 10 — Photomicrograph of nickel-plated fracture surface of HSLA-100 specimen tested at 625°C with a load-on-cooling (449 MPa, t_f = 6 s), 2% Nital, 50X

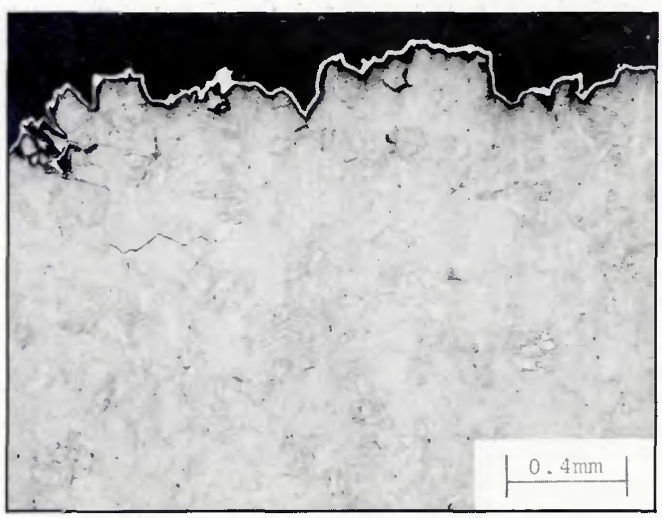

Fig. 11 — Photomicrograph of nickel-plated fracture surface of HSLA-100 specimen tested at 625°C with a load-on-cooling (276 MPa, t_f = 11.7 min.), 2% Nital etch, 50X

graphs at 100X of Type 1 HY-80 and HSLA-100 specimens, respectively, tested under similar conditions (625°C, 483 and 497 MPa). Figure 15 is an SEM fractograph at 1000X of a Type 2 HSLA-100 specimen tested under otherwise similar conditions (625°C, 449 MPa). While low-ductility intergranular fracture was dominant, small areas of localized ductile failure were evident on the fracture surfaces of all three specimens. Some regions of localized ductile failure probably correspond to the triple-point associated transgranular cracking shown in Fig. 12. Other regions of localized plastic deformation appeared to encompass entire grain facets. Some regions of localized plastic deformation also were found to possess a distinctly crystallographic orientation as shown in Fig. 14. The region enclosed in a box in Fig. 14A is shown at higher magnification (1000X) in Fig. 14B. The two lines of localized plastic deformation in Fig. 14B appeared to have a crystallographic orientation, possibly the result of an intersection of a crystallographically oriented feature (lath boundary, twin) with the grain facet.

Fracture surfaces of Types 1 and 2 HSLA-100 test specimens were compared in order to determine what effects, if any, the load-on-cooling had produced. As shown in Figs. 14A and 15, the overall appearance of load and no-load fracture surfaces was very similar. However, inspection of the fracture-surface edges yielded some interesting results. The fracture-surface edges of Types 1 and 2 test specimens are shown in Figs. 16 and 17, respectively. The fracture-surface edge of the Type 1 test specimen (625°C, 497 MPa, t_f = 5 s), shown in Fig. 16, contained a region of extensive ductile rupture approximately 0.6 mm wide. In contrast, the fracture-surface edge of the Type 2 specimen (625°C, 449 MPa, t_f = 6 s), shown in Fig. 17, contained a region of ductile rupture that was only 0.2 to 0.3 mm wide. The origin of these regions may be related to decarburization of the specimen surface during weld simulation and elevated-temperature testing in air. However, the size of the decarburized zone should not differ significantly in two specimens tested under similar time-temperature conditions.

The effect of stress-relief temperature was examined in a direct comparison of HSLA-100 tested at 575°C (435 MPa, t_f = 18.3 min) and 625°C (449 MPa, t_f = 6 s). Fractographs of these specimens are provided in Figs. 18 and 19, respectively. The overall appearance of the two fracture surfaces was very similar but somewhat better detail could be resolved on the grain facets of the 575°C specimen, shown in Fig. 18. Inspection of grain facets at higher magnification revealed no evidence of cavity-mode failure; the fracture morphology of both 575° and 625°C specimens appeared similar to that reported by Shin and McMahon (Ref. 6) to be the result of S-induced, grain-boundary decohesion. However, the presence of sulfur on the fracture surfaces of HSLA-100 or its role in the low-ductility intergranular failure of this material was not confirmed.

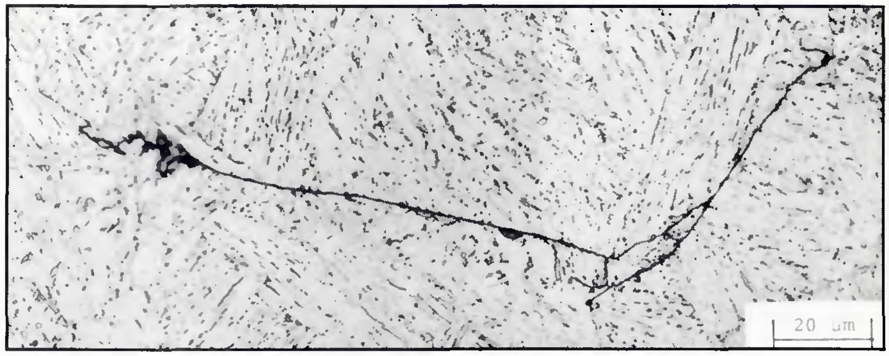

Fig. 12 — Photomicrograph of secondary crack in HSLA-100 specimen tested at 625°C with a load-on-cooling (449 MPa, t_f = 6 s), 2% Nital etch, 1000X

Discussion

Stress-Relief Cracking Test

Measurements of flow stress in the coarse-grained HAZ of HSLA-100 have shown that substantial strengthening occurs during the transformation of unstable austenite to lower-temperature microconstituents. A reasonable fraction (~ 30%) of the room-temperature yield strength is attained only after approximately 50% of the microstructural transformation is complete. Based on these data, a thermomechanical (rather than a thermal) simulation test was developed to model the effect of stress and thermal transients on the stress-relief cracking susceptibility of these steels.

The imposition of mechanical constraint on the cooling portion of the weld thermal cycle resulted in a slight increase in HAZ hardness and stress-relief cracking susceptibility. In explanation of the former, Cohen (Ref. 23) has shown that, for dynamic self-diffusion studies, stress-assisted diffusion occurs if

$$T/T_m \leq 4.9/(2.2 - \log \dot{\epsilon}) \qquad (1)$$

where T = temperature, T_m = absolute melting point, and $\dot{\epsilon}$ = strain rate, in. s^{-1}.

For a $\dot{\epsilon}$ typical of creep deformation (~ 10^{-6} s^{-1}), and rearranging Equation 1, then

$$T \leq 0.6\ T_m \qquad (2)$$

Therefore, for a T_m of approximately 1510°C (2750°F), stress-assisted diffusion[1] can occur at temperatures of 797°C (1466°F) and below.

For the relatively slow cooling rates examined in this study ($t_{800-500}$ = 33 s) and for strain rates typical of localized grain-boundary deformation, it is reasonable to assume that stress-assisted diffusion occurs in Type 2 tests of HSLA-100. The stress-assisted diffusion of Cu and/or carbide-forming elements and the resultant precipitation of Cu-rich clusters and/or alloy carbides during the cooling portion of the thermal cycle would result in increased HAZ hardness. Other mechanisms, such as work hardening resulting from localized plastic flow on cooling,

[1] Cohen (Ref. 23) suggested that the presumption of stress-assisted diffusion be invoked only if plastic deformation increased the diffusion coefficient (D) by a factor of 2 or more.

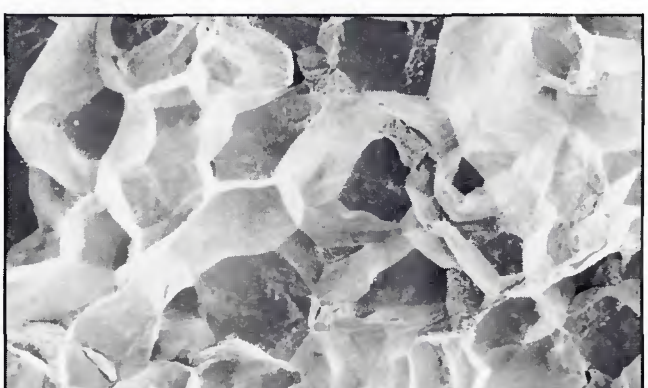

Fig. 13 — SEM fractograph of HY-80 specimen tested at 625°C with no-load-on-cooling (455 MPa, t_f = 1.25 min.)

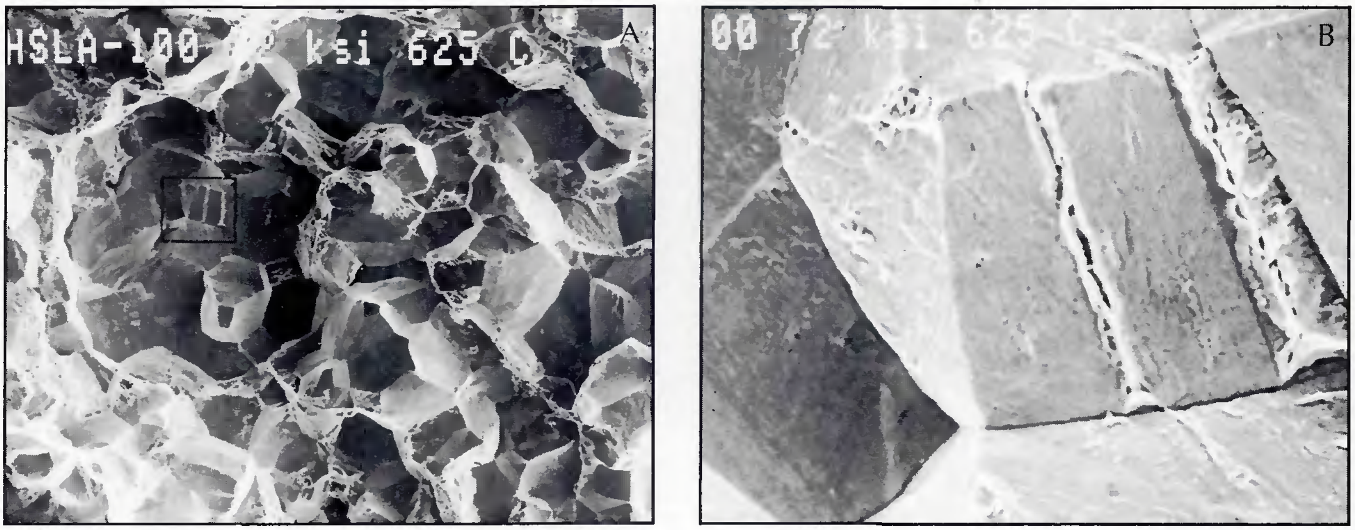

Fig. 14 — SEM fractographs of HSLA-100 specimen tested at 625°C with no-load-on-cooling (497 MPa, t_f = 5 s); A — low-magnification fractograph; B — high-magnification fractograph of region shown in box in A

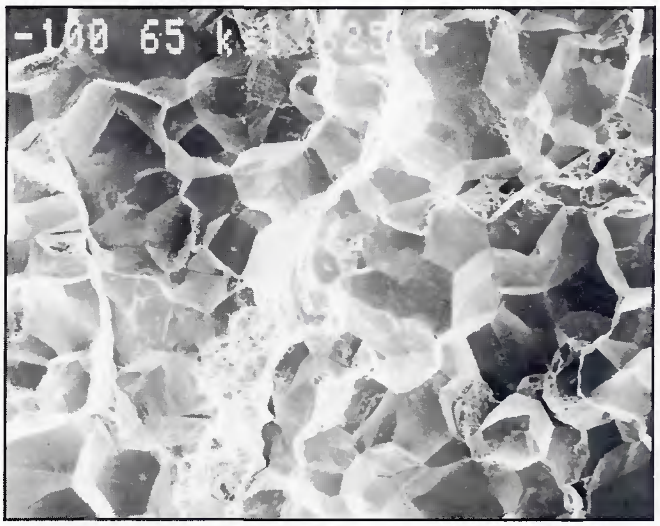

Fig. 15 — SEM fractograph of HSLA-100 specimen tested at 625°C with a load-on-cooling (449 MPa, t_f = 6 s)

Fig. 16 — SEM fractograph of HSLA-100 specimen tested at 625°C with no-load-on-cooling (497 MPa, t_f = 5 s)

Fig. 17 — SEM fractograph of HSLA-100 specimen tested at 625°C with a load-on-cooling (449 MPa, t_f = 6 s)

Fig. 18 — SEM fractograph of HSLA-100 specimen tested at 575°C with a load-on-cooling (435 MPa, t_f = 18.3 min)

Fig. 19 — SEM fractograph of HSLA-100 specimen tested at 625°C with a load-on-cooling (449 MPa, $t_f = 6$ s)

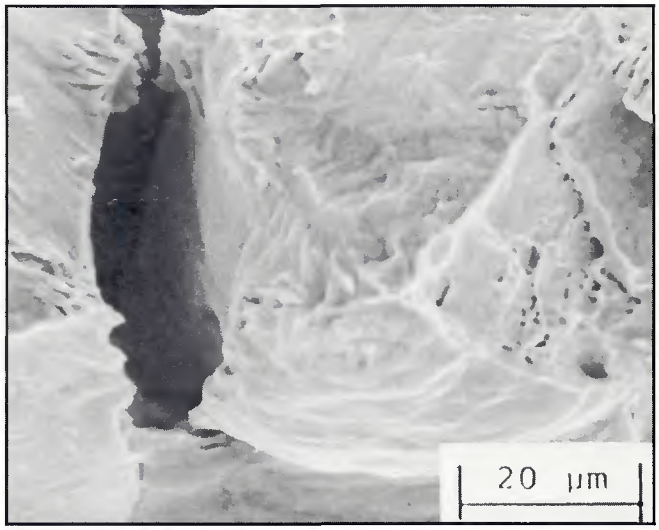

Fig. 20 — SEM fractograph of HSLA-100 tested at 625°C with a load-on-cooling (449 MPa, $t_f = 6$ s), 1200X

may also be involved. The extent to which other mechanisms may be operative, and their contribution to observed increases in HAZ hardness has not yet been determined, but merits study.

The imposition of mechanical constraint on the cooling portion of the simulated weld thermal cycle resulted in only a slight increase in the SRC susceptibility of HSLA-100, as measured by t_f. While it was originally believed that a more significant change in SRC susceptibility would be observed for this alloy, it appears that stress-assisted diffusion/precipitation of Cu or alloy carbides may not be the rate-controlling process for stress-relief embrittlement of HSLA-100 (this will be discussed further in the following section). Further examination of this test technique with respect to alloy systems more sensitive to stress-assisted diffusion should be more informative.

SRC Susceptibility

Vinckier and Pense (Ref. 18), in a study of underclad cracking in pressure-vessel steels, proposed that elevated-temperature (600°C/1112°F) tensile ductilities could be used to evaluate SRC susceptibility as follows: RA < 5% extremely susceptible, RA < 10% susceptible, RA < 15% slightly susceptible, RA > 20% not susceptible.

For identical HAZ simulation and testing conditions, slow-strain-rate tensile ductility would be expected to be equal to or greater than the stress-rupture ductility measured in the present study. Thus, the criteria proposed by Vinckier and Pense should provide a conservative estimate of SRC susceptibility based on ϵ_f measured in stress-rupture tests.

The values of ϵ_f measured for HSLA-100 ranged from 2.4 to 8.9%. For HY-80, the measured values of ϵ_f were 7.3 to 15.8%. As no ϵ_f greater than 10% was reported for HSLA-100, this steel should be classified from "susceptible" to "extremely susceptible" to stress-relief embrittlement. HY-80 should be classified from "slightly susceptible" to "susceptible." For conditions of similar welding parameters, stress-relief temperature, and residual stress, HSLA-100 was more susceptible to stress-relief embrittlement than HY-80. Given the lower S (0.005 versus 0.013 wt-%) and C (0.03 versus 0.18 wt-%) levels and the lower HAZ hardness (HV 284 versus HV 421) of HSLA-100, one might expect it to exhibit better resistance to SRC than HY-80. However, if stress-assisted diffusion of S to the tip of grain-boundary cracks is mainly responsible for embrittlement, as suggested by Shin and McMahon (Ref. 6), the bulk concentration of S in HSLA-100 (50 ppm) is more than sufficient to produce at least a monolayer at the boundaries of a grain-coarsened HAZ. Sun, *et al.* (Ref. 5), has reported that, in the presence of a very small amount of B (~ 2 ppm), only a few ppm of S are necessary for high SRC susceptibility.

Despite the aforementioned difference in HAZ hardness, the differential strengthening of grain interiors relative to grain boundaries may be greater in the Cu-containing HSLA-100 than in HY-80. As a result, greater strain concentration at the boundaries would occur in the HSLA steel; this would result in decreased t_f and ϵ_f for this material. Additionally, as a result of microalloying additions to HSLA-100, there may be other embrittling mechanisms, such as NbC or Nb(CN) precipitation on grain boundaries; these would further increase the SRC susceptibility of HSLA-100 relative to HY-80. The microalloying additions do result in a somewhat finer grain size in the HAZ of the HSLA steel. Because a fraction of t_f in the creep-rupture process is comprised of facet-sized cracks linking to form a macrocrack of critical size, a smaller grain size should result in a greater t_f (Ref. 24). If the HAZ grain size of HY-80 and HSLA-100 were equivalent, the SRC susceptibility of HSLA-100 would be further increased relative to that of HY-80.

Metallographic and Fractographic Results

Stress-rupture tests of simulated heat-affected zones in HY-80 (no-load-on-cooling), HSLA-100 (no-load-on-cooling), and HSLA-100 (load-on-cooling) resulted in low-ductility intergranular fracture characteristic of stress-relief embrittlement. Fractography of both alloys, tested under a variety of conditions, revealed no evidence of cavity-mode failure on intergranular facets. Varying degrees of localized plastic deformation were observed on all fracture surfaces (Figs. 13–15). Similar results have been reported in previous investigations of Cu-containing HSLA steels (Ref. 4). While the origin of these regions is unclear, they may result from ductile overload of grain facets which, for reasons of orientation, size, or segregation, did not have adequate concentrations of segregated S to engender grain-boundary decohesion. Probable evidence of this is shown in Fig. 20; an otherwise smooth grain facet, the result of brittle failure by decohesion, displays small areas of ductile overload (indicated with arrows). Similarly, the origin of ductile rupture regions near fracture-surface edges (Figs. 16 and 17) is also unclear, although some relationship appears to exist between the extent of these regions and the presence of mechanical constraint on cooling.

The extensive secondary cracking observed in HY-80 (Fig. 8) suggests that SRC in this alloy is propagation-con-

Table 4—Comparison of Calculated Activation Energies with Diffusional Data

Process	Activation Energy (kcal/mol)	Temperature Range (°C)	Reference
SRC of HY-80	~78	593-625	–
SRC of HSLA-100	~91	575-625	–
LDIGF of 2¼-1 Mo steel (0.006 S, 0.031 P)	~83	550-650	10
LDIGF of 2¼-1 Mo steel (0.014 S, 0.010 P)	~63	500-650	10
Grain-Boundary Diffusion			
Fe in pure Fe	22.0	550-810	28
Fe in Fe + 100 ppm P	34-46	550-810	28
Bulk Diffusion			
C in Fe	29.3	616-844	29
P in Fe	72-86	527-727	30
P in Fe-0.1P	68.8	Ferromag[a]	31
P in Fe-0.29Mo-0.1P	104	Ferromag[a]	31
P in Fe-1.03Ni-0.1P	80.3	Ferromag[a]	31
S in Fe	48.9	750-900	32
S in Fe	55.3	700-900	33
Cr in Fe	57.5	775-875	34
Fe in Fe	68-72	640-810	28
Ni in Fe	58.7	600-680	35
Cu in Fe	62.5	700-759	36
Nb in Fe	60.0	750-890	37
Mo in Fe	73.0	750-875	38

(a) Temperature range not specified.

trolled, *i.e.,* a number of cracks may nucleate before linkage and growth to a critical size occurs and results in failure. Similar observations of secondary cracking in HY-80 were reported in a previous investigation (Ref. 25). Relatively little secondary cracking was observed in HSLA-100; however, the presence of mechanical constraint on cooling and stress-rupture testing at lower stresses (longer t_f) slightly increased the amount of secondary cracking. This suggests that SRC in HSLA-100 is nearly initiation-controlled, and relatively few cracks need to be initiated before linkage occurs and the critical size for failure is obtained.

Mechanisms

Interpretation of the most recent results of Lewandowski, *et al.* (Refs. 9, 10), and Sun, *et al.* (Ref. 5), in combination with established literature on stress-relief cracking (Refs. 1-3, 5, 6, 12-14, 16, 17), suggests that two processes are necessary for stress-relief embrittlement of the coarse-grained HAZ in ferritic steels:

1) The segregation of embrittling species, most notably S, to grain-boundary surfaces, and

2) The strengthening of grain interiors relative to grain boundaries.

It can be postulated that both of the aforementioned processes will be thermally activated and will, therefore, display an exponential dependence on temperature. It then follows that calculation of an activation energy for embrittlement based on the results of SRC tests should give an indication of the thermal-activation requirements of the rate-limiting step in the embrittlement process.

The results of Type 2 tests shown in Fig. 7B. were used to estimate the activation energy for stress-relief cracking in HSLA-100 for $t_f > 1$ min. Stress-rupture data from a previous investigation (Ref. 26), shown in Fig. 7A, were utilized in conjunction with data from Type 1 tests to estimate the activation energy for HY-80. Williams (Ref. 27) has shown that, for environmental-assisted cracking, the dependence of crack growth rate on temperature can be described as

$$da/dt = A_1 e^{-Q/RT} \tag{3}$$

If it is assumed that one failure mechanism is operating and that da/dt is constant for any test, then

$$t_f = A_2 e^{Q/RT} \tag{4}$$

When Equation 4 is used, the activation energy (Q) calculated for HSLA-100 is 91 kcal/mol, and the Q calculated for HY-80 is 78 kcal/mol. It must be noted that, since no crack growth rates were measured in this study and since activation energies were calculated from linear regression fits of relatively limited data, these values can be used only as approximations of thermal activation requirements. Nonetheless, the approximate values of Q can be used to speculate regarding the rate-controlling mechanism of stress-relief cracking for these alloys.

The activation energies calculated for stress-relief cracking of HY-80 and HSLA-100 are shown in Table 4 along with similar values for 2¼ Cr-1 Mo steels and for a variety of diffusing species in Fe. These data indicate that the activation energies calculated for SRC of HY-80 and HSLA-100 are on the order of those for bulk substitutional diffusion in Fe. The activation energies shown in Table 4 for low-ductility intergranular failure (LDIGF) of a 2¼ Cr-1 Mo steel were calculated by Lewandowski, Hippsley and Knott (Ref. 10) from the results of stress-relaxation crack-growth rate experiments using a more rigorous dependence of crack-growth rate on temperature and stress intensity. It is interesting to note, however, the similarity between values of Q calculated for the 2¼ Cr-1 Mo steel, HY-80, and, to a lesser extent, HSLA-100. It should be noted that, wherever possible, activation energies reported in Table 4 are for temperature ranges relevant to the stress-relief treatments simulated in this investigation, *i.e.,* 575° to 625°C. This is significant because activation energies for substitutional bulk diffusion in Fe below the Curie temperature have been reported to be somewhat greater than those for higher temperatures as a result of ferromagnetic ordering effects (Refs. 31, 32, 36).

The three calculated values of Q are significantly greater than the cited values of Q for interstitial bulk diffusion and grain-boundary self-diffusion in Fe. For this reason, it is reasonable to assume that the rate-controlling process in SRC is related to substitutional diffusion in Fe. Because of the scatter inherent in diffusion data and the approximate nature of the activation energies calculated in this and other investigations, it was difficult to isolate the diffusion of a particular solute as the rate-controlling step in stress-relief embrittlement. However, it is instructive to examine the relationship between values of Q calculated in this study and by Lewandowski, Hippsley and Knott (Ref. 10) and the values of Q for bulk diffusion in Fe. Of the solutes shown in Table 4, it appears that the activation energies cited for bulk diffusion of P, Fe and Mo in Fe are closest in magnitude to the approximate activation energies calculated for stress-relief embrittlement. Two values of Q for bulk diffusion of S in Fe, from the oft-cited work of Ainslie and Seybolt (Ref. 32) and from a more recent study by Gruzin (Ref. 33), are listed in Table 4. Both are significantly less than the approximate activation energies calculated for HY-80, HSLA-100 and LDIGF of the high-P 2¼ Cr-1 Mo steel. This would appear to support the suggestion by Lewandowski, Hippsley and Knott (Ref. 10) that stress-assisted diffusion of S causes grain-boundary decohesion but is not the rate-controlling process. It is interesting to note that the activation energies for diffusion of P in Fe-0.29 Mo and Fe-1.03 Ni alloys, 104 and 80.3 kcal/mol, respectively, nearly bracket the activation energies calculated for stress-relief embrittlement of HY-80, HSLA-100 and high-P 2¼ Cr-1 Mo steels. Lewandowski, Hippsley and Knott (Ref. 10) did not consider the activation energies for diffusion of Mo in Fe and P in Fe and Fe-base alloys.

It should also be noted that for the high-stress ($\sigma \geq 400$ MPa/58 ksi) tests conducted in this investigation, where t_f was 1 min or less, it is unlikely that embrittling species could diffuse significant distances at these relatively low temperatures. It is possible that some segregation of embrittling species occurs during the weld thermal cycle. However, activation energies calculated from SRC tests would not reflect the diffusion of these species during short time tests or prior weld thermal transients. This may be reflected in the change in slope of log σ versus log t_f results at 400 MPa ($t_f \sim 1$ min), as reported in Fig. 7B. Calculation of Q at higher stresses yields considerably higher values.

Lewandowski, Hippsley and Knott (Ref. 10) have suggested that, while stress-assisted diffusion of S ahead of growing cracks was necessary, it was the displacement of Fe atoms from the crack tip, via self diffusion, which was most likely the rate-controlling process. The diffusion of Fe atoms away from the crack tip would engender vacancy flow towards the crack tip, *i.e.,* diffusional creep. Thus, it appears that diffusional creep, accentuated by precipitation strengthening of grain interiors, is the rate-controlling process and, therefore, directly affects t_f. Stress-assisted diffusion of S acts to reduce the cohesive strength of grain boundaries; this indirectly affects t_f by reducing the σ required for failure. More accurate estimates of Q for stress-relief embrittlement and better characterization of diffusion of relevant solutes in engineering alloys will be needed before the mechanisms of SRC can be described more accurately.

Summary

A preliminary study of the effects of mechanical constraint on cooling in the coarse-grained HAZ of an experimental Cu-containing HSLA steel has been conducted. A modified HAZ simulation stress-relief cracking test was developed, which also simulates the increasing residual stress present on cooling in a weldment. While this study was by no means exhaustive, interesting observations have been made. The stress-relief cracking susceptibility of the low-carbon HSLA steel was greater than that of the higher-carbon, quench-and-tempered, high-yield-strength steel. The imposition of mechanical constraint on the cooling portion of the weld thermal cycle slightly increased the HAZ hardness and the stress-relief cracking susceptibility, as measured by t_f, of the HSLA steel. Calculation of approximate activation energies and comparison with similar data for 2¼ Cr-1 Mo steel suggest that Lewandowski's model, involving the bulk self diffusion of iron away from propagating crack tips in embrittled grain boundaries as the rate-controlling process, may be appropriate for these alloys.

Clearly, more work is necessary before the effect of mechanical constraint on stress-relief embrittlement can be effectively modeled. Careful Auger electron spectroscopy and scanning-transmission electron microscopy studies are required to define the roles of copper precipitation, grain-boundary precipitation, and impurity segregation in stress-relief embrittlement of HSLA steels.

Conclusions

The stress-relief cracking susceptibility of an experimental heat of HSLA-100 and a production heat of HY-80 was examined using a thermomechanical heat-affected zone simulation test.

1) Experimental heat of HSLA-100 was, under similar conditions, more susceptible to stress-relief cracking than HY-80.

2) Measurements of HAZ flow stress indicate that a large increase in residual stress level can occur only after transformation of unstable austenite to lower-temperature microconstituents is approximately 50% complete.

3) At stresses greater than 400 MPa (58 ksi), the stress-relief cracking susceptibility of simulated heat-affected zones in HSLA-100 was increased only slightly by the imposition of mechanical constraint on cooling from the peak temperature.

4) The rate-controlling process in the stress-relief embrittlement of these alloys appears to have thermal activation requirements similar to those of substitutional bulk diffusion, possibly self diffusion, in the steel matrix.

Acknowledgments

The authors would like to acknowledge the material and financial support contributed by Molycorp, Inc.

References

1. Meitzner, C. F. 1975. *WRC Bulletin No. 211,* Nov.
2. Dix, A. W., and Savage, W. F. 1973. *Welding Journal* 52(3):135-s to 139-s.
3. Thamburaj, R., Wallace, W., and Goldak, J. A. 1983. *Intl. Met. Rev.* 28(1).
4. Lundin, C. D., Menon, R., and Chen, Z. 1986. *Advances in Welding Science and Technology,* ASM: Metals Park, Ohio, pp. 559.
5. Sun, J., *et al.* 1987. *Matls. Sci. and Tech.* 3(2):139–145.
6. Shin, J., and McMahon, C. J., Jr. 1984. *Acta. Met.* 32(9):1535–1552.
7. Troiano, A. R. 1960. *Trans. ASM,* 52:54–80.
8. Hippsley, C. A., Rauh, H., and Bullough, R. 1984. *Acta. Met.* 32(9):1381–1394.
9. Lewandowski, J. J., *et al.* 1987. *Acta. Met.* 35(3):593–608.
10. Lewandowski, J. J., Hippsley, C. A., and Knott, J. F. 1987. *Acta. Met.,* 35(8):2081–2090.
11. Druce, S. G., Gage, G., and Jordan, G. 1986. *Acta. Met.* 34(4):641–652.
12. Emmer, L. G., Clauser, C. D., and Low, J. R., Jr. 1973. *WRC Bulletin No. 183,* p. 25.
13. Bentley, K. P. 1964. *Brit. Weld. J.* 11(10):507–515.
14. Meitzner, C. F., and Pense, A. W. 1969. *Welding Journal* 48(10):431-s to 440-s.
15. Rosenstein, A. H. 1970. *Welding Journal* 49(3):122-s to 131-s.
16. Visbisky, K., Somers, B. R., and Pense, A. W. 1986. *Welding Research: The State of the Art,* ASM: Metals Park, Ohio, pp. 187.
17. Duvall, D. S., and Owczarski, W. A. 1969. *Welding Journal* 48(10):10-s to 22-s.
18. Vinckier, A. G., and Pense, A. W. 1974. *WRC Bulletin No. 197.*
19. Miglin, M. T., Hirth, J. P., and Rosenfield, A. R. 1983. *Met. Trans.,* 14A(10):2055–2061.
20. ASTM A710-79, 1979.
21. *Military Specification for Steel Plate, Alloy, Structural, High Yield Strength (HY-80 and HY-100),* MIL-S-16216J (SH), 10 April, 1981.
22. Balaguer, J. P., Wang, Z., and Nippes, E. F. 1987. Rensselaer Polytechnic Institute, Unpublished research.
23. Cohen, M. 1970. *Trans. JIM,* 11(3):145–151.
24. Dyson, B. F., and Taplin, D. M. R. 1976. *Grain Boundaries.* Institute of Metallurgists Series, 3(5):23.
25. Debarbadillo, J. J., Pense, A. W., and Stout, R. D. 1966. *Welding Journal* 45(8):357-s to 367-s.
26. Ledman, J. L., Lundin, C. D., and Savage, W. F. 1963. *Study of the Transformational Characteristics and the Weldability of HY-80 Steel,* R.P.I. Final Technical Report No. SR007 01 01.
27. Williams, D. P. 1973. *Intl. J. Fracture* 9(3):63–73.
28. Hänsel, H., *et al.* 1985. *Acta. Met.,* 33(4):659–665.
29. Homan, C. G. 1964. *Acta. Met.* 12(9):1071–1079.
30. Luckman, J. G. 1981. *Dissert. Abs. Intl.* 42(3):124.
31. Matsyama, T., Hosokama, H., and Suto, H. 1983. *Trans. JIM* 24(8):589–594.
32. Ainslie, N. G., and Seybolt, A. U. 1960. *J. Iron and Steel Inst.* 194(3):341–350.
33. Gruzin, P. L., Mural, V. V., and Fokin, A. P. 1972. *Phys. Met. Metallog.* 34(6):209–212.
34. Huntz, A. M., Aucouturier, M., and Lacombe, P. 1967. *C. R. Acad. Sci. Paris Ser. C.* 265(10):554.
35. Hirano, K., Cohen, M., and Averbach, B. 1961. *Acta. Met.* 9(5):440–445.
36. Speich, G. R., Gula, J. A., and Fisher, R. M. 1966. *The Electron Microprobe,* New York: John Wiley, pp. 525–542.
37. Geise, J., and Herzig, C. 1985. *Zeit. Metall.* 76(9):622–626.
38. Borisov, V. T., Golikov, V. M., and Shcherbedinski, G. V. 1966. *Fiz. Metal. i Metalloved* 22(1):159.